

Effects of doping on charge-density waves in layer compounds

F. J. Di Salvo, J. A. Wilson, B. G. Bagley, and J. V. Waszczak

Bell Laboratories, Murray Hill, New Jersey 07974

(Received 3 April 1975)

Electrical, magnetic, and thermal properties of $1T$ -TaS₂ and $1T$ -TaSe₂ doped with cations (Ti, Zr, Hf, V, Nb), $1T$ -Nb_{1-x}Ti_xS₂/Se, and $1T$ -TaS_{2-x}Se_x are reported, with particular emphasis on the effects of doping on the charge density wave (CDW) observed in the parent compounds. Cation doping is found to slightly suppress the onset temperature T_0 of the CDW, but to suppress much more rapidly the lock-in to the commensurate state at T_d . Beyond a doping level of $\approx 10\%$ the commensurate state no longer exists. The anion disorder in $1T$ -TaS_{2-x}Se_x, on the other hand, does not suppress transitions toward the commensurate state at any x . An anomalous increase of the low-temperature resistivity is observed for some compounds at certain doping levels. This increase appears to be due to *both* a reduction in carrier density and a reduction in mobility. The data are qualitatively consistent with recent ideas concerning the role of electronegativity in lock-in of the CDW to the commensurate state, and recent Landau models of the CDW state.

I. INTRODUCTION

Within the last few years, it has become apparent that many of the layered compounds having metallic conductivity exhibit electronic instabilities.^{1,2} Because the details concerning the existence of the instability have just recently been published,² a short description is necessary here to introduce nomenclature and several parameters. The instability is due to a Fermi-surface-driven charge density wave (CDW). A CDW consists of a periodic variation in the conduction-electron density having a wave vector of magnitude q_0 and a static periodic distortion of the lattice at the same q_0 . \vec{q}_0 is determined, at least over some temperature interval, by a particular spanning vector of the Fermi surface (FS), for which the electronic susceptibility $\chi(\vec{q}_0)$ diverges (this susceptibility includes all electron-electron and electron-phonon interactions, as distinct from the "bare" susceptibility $\chi^0(\vec{q}_0)$ for free noninteracting electrons). Since the lattice is also distorted, x-ray, electron, or neutron diffraction shows peaks at $\vec{G} \pm n\vec{q}_0$, and thus \vec{q}_0 can be simply determined. (\vec{G} is a reciprocal-lattice vector of the undistorted state, and n is any integer.)

The metallic compounds of the layered transition-metal dichalcogenides can be prepared in a number of polymorphic layered structures.³ In this report, we shall discuss the properties of compounds and alloys of the $1T$ structure type. The $1T$ structure, when the q_0 distortion is absent or neglected, is of the CdI₂ type, the simplest of the hexagonal layered structures (see, for example, Ref. 3). This structure has one formula unit per unit cell, the layers being formed from sandwiches three atoms thick. The middle sheet (metal atoms) is in octahedral holes formed by

the top and bottom sheets of close-packed chalcogen atoms. While bonding within a sandwich is strong, that between sandwiches is of the weak van der Waals type, leading to a marked two-dimensional anisotropy of the physical properties.

The $1T$ compounds show an undistorted structure at high temperatures. As the temperature is reduced below an onset temperature, T_0 , satellite spots at three symmetry-related q_0 's and their multiples appear, along with considerable diffuse scattering. In general, \vec{q}_0 is incommensurate with the lattice spacings, that is, it is not a simple small integer fraction of a reciprocal-lattice vector \vec{G} . Having measured \vec{q}_0 , the important spanned sections of the FS can be identified by comparison with band calculations.⁴ As the temperature is further reduced, the amplitude of the CDW increases, until at T_d the CDW locks into a commensurate geometry in a first-order transition, i.e., a superlattice forms, by a slight change of the magnitude of \vec{q}_0 and/or a change in the direction of \vec{q}_0 . This lock-in transition is essentially a local effect (not *primarily* determined by the Fermi surface). When commensurate, the charge maxima are all placed on cation sites, further reducing Coulomb and elastic energies of the CDW. The magnitude of the atomic displacements are on the order of 0.05 to 0.25 Å, or a few percent of an interatomic distance. These static displacements are similar to the thermal displacements expected near T_d . The intensity of satellite peaks at $\vec{G} + \vec{q}_0$ is thus quite weak compared to the main Bragg peaks at \vec{G} . In light of these facts, we may describe the distortions as small; however, the effect of the CDW on the electronic properties can be quite large.

Besides illustrating the generality of the CDW instability in these $1T$ compounds, this study

enables us to separate the effect of the Fermi surface of the alloys (in the rigid-band approximation) on T_0 and T_d from that of potential disorder and to further understand the nature of these CDW instabilities. In this paper we report the properties of a number of $1T$ compounds, these systems include: $1T$ - $Ta_{1-x}M_xS_2$ with $M = Ti, Zr, Hf, Nb, V$; $1T$ - $Ta_{1-x}M_xSe_2$ with $M = Ti, Zr$; $1T$ - $Nb_{1-x}Ti_xSe_2$; and $1T$ - $TaS_{2-x}Se_x$. Other systems, which were only cursorily examined or which failed to form in the $1T$ phase, will be mentioned.

Overhauser first proposed the existence of the CDW state in metals in 1968.⁵ Overhauser originally proposed that electron-electron and electron-phonon interactions could produce a divergence in $\chi(\vec{q})$, independent of the FS shape [i.e., independent of $\chi^0(\vec{q})$]. Many theorists believe, however, that both a peak in $\chi^0(\vec{q})$ and many-body interactions are required for the CDW state to occur. Since experimental observation of the CDW state is so recent, a complete account of the physical properties of CDW systems may be helpful in untangling these theoretical questions. We should note here, however, that $\chi^0(\vec{q})$ in these systems is expected to have a peak because of the near two-dimensional nature of the FS. Recent calculations bear this out.⁶ No experimental data presently shows the existence of a CDW in metals with a near spherical FS, where $\chi^0(\vec{q})$ decreases monotonically for increasing q_0 . One might ask: If a peak in $\chi^0(\vec{q})$ is necessary, how large must it be? Hopefully, experiments on these and as yet to be discovered CDW systems will help answer these questions.

II. SAMPLE PREPARATION

The starting metals were powders of 99.95% purity or better, while the S, Se, or Te were 99.999% pure. Generally, stoichiometric mixtures of the appropriate compound (weighed to the nearest mg) of approximately 5 g total weight were sealed in small quartz tubes under vacuum (10 mTorr or less), and reacted for several days between 800° to 1000°C. Pure $1T$ - TaS_2 and $1T$ - $TaSe_2$ powders were prepared with excess chalcogen and quenched into cold water from above 750 or 950°C, respectively, as previously described.^{7,8} Since the $1T$ polymorph of the pure compounds is metastable, quenching is necessary. Interpolymorphic transformation of these pure $1T$ materials readily occurs when they are heated to 200–250°C.

Those samples containing two different cations were opened after the initial reaction, ground, pressed into pellets at 50 000 psi, and resealed

in quartz tubes with enough excess chalcogen to give approximately 1–2 atm vapor pressure at 900–1000°C. (i.e., for S, ≈ 1 to 2 mg/cm³ of internal tube volume, or for Se, ≈ 2 to 4 mg/cm³). These samples were reheated to ≈ 900 – 1000 °C for 5–10 days, so that diffusion of the cations could occur producing essentially homogeneous pellets. The samples were usually air quenched, the excess chalcogen condensing on the tube walls. In most cases, the weight of this condensed excess was within several milligrams of the excess added to the tube.

Magnetic susceptibility measurements were performed on powder samples by crushing the pellets obtained after homogenizing. Single crystals were used for electrical, thermal, or electron microscopy measurements.

Single crystals were prepared by iodine vapor transport [≈ 5 (mg I)/cm³] in closed quartz tubes, usually 16 mm i.d. and 200 mm long. This technique is described elsewhere.^{6,7} Again, for crystal growth, excess chalcogen is usually added to the transport tube (S, ≈ 1 to 2 mg/cm³, Se, ≈ 2 to 4 mg/cm³). The growth temperature was usually 750°C for the sulfide compounds or 900–950°C for the selenides. The temperature gradient between the (hotter) starting powder and the growth zone was between 50 and 100°C. In most cases, complete transport of the starting material occurred in 7–10 days or less, after which the tubes were rapidly quenched into cold water to insure retention of the $1T$ phase. Crystals of $1T$ - TaS_2 and $1T$ - $TaSe_2$ produced by this method are known to be stoichiometric to within at least 0.5%, even though the growth takes place in a chalcogen atmosphere.⁷ Several of the alloys, usually at a large doping level (x) for each doping cation, were burned in an oxygen atmosphere on a Dupont thermogravimetric analyzer (TGA) and were stoichiometric to $\pm 1\%$. The larger uncertainty here arises in part from some uncertainty in x in the crystals (see later text).

Crystals of $1T$ - $TaS_{2-x}Se_x$ were grown from powder directly after the initial reaction step. Excess S and Se in the molar ratio $2-x$ to x was added to give pressures at 950°C of 1–2 atm. Phase separation of $1T$ powders for $x > 0.4$ previously observed⁹ did not occur when single crystals were prepared.

In some cases, the stoichiometric $1T$ phase could be prepared and retained at room temperature only over a certain range of x . $1T$ - $Nb_{1-x}Ti_xSe_2$ was obtained only for $x \geq 0.06$ and $1T$ - $Nb_{1-x}Ti_xS_2$ for $x \geq 0.04$. $1T$ - $TaSe_{2-x}Te_x$ could not be prepared in *pure form*, even for x as small as 0.1. The presence of the $1T$ phase (and absence of other polymorphs) was always confirmed by x-ray dif-

fraction. In all cases, confirmation of pure $1T$ phase was assured if the crystals had smooth basal plane surfaces, cleaved easily parallel to the layers, and had the proper color. The $1T$ polymorphs have either a yellow bronze or purple bronze color, whereas all other polymorphs of TaS_2 , $TaSe_2$, or $NbSe_2$ have either silvery or blue-black metallic luster. In other cases, substitution of Ta by the intended doping cation did not occur. These include Sn, Ge, and Si with the maximum possible solubility (limit of detection) $\approx 0.2\%$. Other cations, specifically Cr, Mn, Co, Fe, Ni will substitute for Ta, but these elements appear to be divalent, driving the Ta to the pentavalent state. The properties of these compounds will be reported elsewhere.

Each batch of crystals was studied by x-ray fluorescence to verify that the dopant was indeed included in the crystals at the desired level. In most cases, the homogenized pellets prepared prior to crystal growth were used as standards, and the ratio of dopant signal to Ta or Nb signal increased smoothly vs x . In some growth tubes, the concentration of dopant measured by fluorescence analysis was the same from crystal to crystal ($\pm 5\%$ dopant), but in others the concentrations differed by as much as 25% (for cation doping—usually at low levels). In all cases, the concentration used, when plotting the variation of physical properties vs x , is that determined by fluorescence analysis on the same crystal used for that particular measurement.

The $1T$ polymorph of Nb or Ta is stabilized over the entire temperature range studied (4.2–1000 °K) when doped beyond ≈ 5 to 6% with group-IV cations. Cation mixing of Nb and Ta did not enhance the stability of pure $1T$ - TaS_2 . Pure $1T$ - $NbSe_2$ cannot be retained at room temperature, and $1T$ - NbS_2 has not been observed at any temperature.

III. MEASUREMENTS

Electrical resistivity parallel to the layers (ρ) was measured on single crystals by the four-probe technique. The thin crystals were carefully cut into an approximately rectangular shape, usual dimensions were $10 \times 2.5 \times (0.05 \text{ to } 0.2) \text{ mm}^3$ (thickness). Silverpaste contacts were lapped over the edges of the crystal to make contact with all the layers. While this four-probe method can lead to difficulties, especially if there is a break between layers effectively isolating one section electrically from another, several crystals examined by the Van der Pauw technique¹⁰ gave the same results. However, uncertainties in the *absolute* accuracy of the resistivity as large as 15% are expected, since the thickness of the crystals was usually

not uniform and the silver-paste voltage contacts were approximately 0.5 mm wide.

Usually, ρ vs temperature was obtained by cooling from room temperature to 4.2 °K at 2–3 °K/min (slower below 30 °K) and then reheating at the same rate to ≈ 375 °K and then back to room temperature. Such cycling insured that changes seen vs temperature were not due to contacts breaking away from portions of the crystal (as occasionally happened). Resistivity measurements above 375 °K were performed by making four pressure contacts to the crystal with Pt–10-at.% Rh wire and were carried out in a high-purity Ar atmosphere.

Magnetic susceptibility (χ_g) was measured on a number of powder samples from 4.2 to 900 °K using the Faraday technique. Calibration and accuracy of our apparatus are described elsewhere.¹¹ Relative changes in χ_g vs temperature of $5 \times 10^{-10} \text{ emu/g}$ could be detected, but the absolute accuracy of the susceptibility compared to several standards is $\pm 2\%$. No attempts were made to prove random orientation of the powder to insure measurement of the average susceptibility in these anisotropic systems. However, in a number of studies on pure TaS_2 , the susceptibility determined from powder was equal to the correctly averaged single-crystal measurements.¹² Evidently, the grains of powder often include many crystallites whose orientations are close to random.

Electron-diffraction measurements were performed at 200 kV on a Jeol 200 electron microscope. The details are described in a previous article.²

Differential-scanning-calorimetry (DSC) measurements were obtained with a Perkin-Elmer scanning calorimeter. Again the accuracies and calibration of this apparatus are described elsewhere.⁷

IV. RESULTS

In this section we first review the properties of $1T$ - TaS_2 and $1T$ - $TaSe_2$ as a basis for discussion of the changes wrought by doping. Then we consider the case of doping $1T$ - TaS_2 with Ti, since we have obtained the most data in this system. We finally consider the remaining systems in sequence. Table I summarizes the most important aspects of this section.

A. $1T$ - TaS_2 and $1T$ - $TaSe_2$

ρ and χ for $1T$ - TaS_2 and $1T$ - $TaSe_2$ are shown in Figs. 1 and 2, respectively, and compared to the room-temperature stable $2H$ polymorphs. While the decrease in ρ and χ in the $2H$ polymorphs at low temperatures is known to also coincide with CDW formation,^{1,2} it is clear that the metallic

TABLE I. List of compounds studied with CDW onset temperature T_0 , commensurate transition temperature T_d , the almost commensurate transition temperature T'_d , and comments. For the alloys we list the rates of change of T_0 , T_d , and T'_d vs x and the critical concentration (x_c), beyond which the transitions at T_d and T'_d are absent. Dots in the appropriate space indicate not enough data available to specify.

Compounds	T_0 (K)	T_d (K)	T'_d (K)	Comments	
1T-TaS ₂	≈600	≈200	352	$\Delta H_d = 18 \frac{\text{cal}}{\text{mole}}$, $\Delta H'_d = 123 \frac{\text{cal}}{\text{mole}}$	
1T-TaSe ₂	≈600	473	none	$\Delta H_d = 374 \frac{\text{cal}}{\text{mole}}$	
Compounds	dT_0/dx (K/at.%)	dT_d/dx (K/at.%)	dT'_d/dx (K/at.%)	x_c	Comments
1T-Ta _{1-x} Ti _x S ₂	≈3	T_d eliminated for $x \geq 0.005$	10	0.15	$\Delta H'_d$ initially rises with x
1T-Ta _{1-x} Nb _x S ₂	...	T_d eliminated for $x \geq 0.005$	≈12	0.10	$\Delta H'_d$ initially falls with x
1T-Ta _{1-x} V _x S ₂	...	T_d rapidly eliminated	≈12	0.10	
1T-Ta _{1-x} Hf _x S ₂	...	T_d rapidly eliminated	...	<0.08	Only $x=0.085$ studied
1T-Ta _{1-x} W _x S ₂	...	T_d rapidly eliminated	≈17	...	Estimate max W included at $x=0.01$
1T-Nb _{1-x} Ti _x S ₂	No electrical data obtained
1T-Ta _{1-x} Ti _x Se ₂	...	13	Not present	0.10	ΔH_d falls linearly with x
1T-Ta _{1-x} Zr _x Se ₂	...	18	Not present	0.08	ΔH_d falls linearly with x
1T-Nb _{1-x} Ti _x Se ₂	...	≈20	Not present	0.08	
1T-TaS _{2-x} Se _x	...	See text and Fig. 24		does not apply	Transitions toward commensurate state occur at all x

state is considerably more perturbed by the CDW in the 1T case.

1T-TaSe₂ shows an incommensurate CDW below $T_0 \approx 600$ °K and above the first-order transition at $T_d = 473$ °K.^{1,8} This CDW is built from three symmetry-related \vec{q}_0 waves (each rotated 120° about the hexagonal crystal c_0 axis) where $\vec{q}_0 = \vec{q}'_0 + \frac{1}{3}\vec{c}_0^*$ with \vec{q}'_0 the basal-plane projection of \vec{q}_0 , and where the asterisk indicates a primary reciprocal-lattice vector. The component along \vec{c}_0^* shows that the CDW's do not stack directly on top of one another from layer to layer, but in a simple ABC sequence. For 1T-TaSe₂ with $T \geq T_d$, $|\vec{q}_0| = 0.682 \text{ \AA}^{-1}$ ($\vec{q}'_0 \approx 0.285 \vec{a}_0^*$). At T_d , the lock-in or superlattice temperature \vec{q}'_0 rotates from parallel to \vec{a}_0^* to 13°54' away from \vec{a}_0^* and shrinks by 2.5% to become a "3×1" superlattice in a hexagonal array with $a = (13)^{1/2}a_0$. Further, Moncton and Axe¹³ have shown that $c = 13c_0$ below T_d , i.e., the component of \vec{q}_0 perpendicular to layers is a multiple of $\frac{1}{13}c_0^*$.

Above T_d (in the incommensurate state), ρ is higher and χ is lower than expected for the undistorted 1T phase (compare to 2H phase), since the normal FS is disrupted, gaps being introduced near those portions of the FS spanned by \vec{q}_0 . Below

T_d the gaps increase (cover more FS and/or become larger) so that ρ increases and χ decreases. The metalliclike conductivity at low T comes from those portions of the FS not removed by gap formation (compare ρ of 1T and 2H, estimate 10% left). Alternately, below T_d we could say a smaller Brillouin Zone (BZ) is defined by the superlattice, and the bands are folded back into the new BZ leaving mostly full bands.

The case of 1T-TaS₂ is somewhat more complicated because two first-order transitions are seen. When $352 \text{ °K} < T < 600 \text{ °K}$, the extra satellite reflections indicate a state essentially identical to that of 1T-TaSe₂ above T_d . Again $\vec{q}_0 = \vec{q}'_0 + \frac{1}{3}\vec{c}_0^*$ with $\vec{q}'_0 \approx 0.288 \vec{a}_0^*$. However, when $200 \text{ °K} \lesssim T < 352 \text{ °K}$, a novel state appears. In this case \vec{q}'_0 rotates by approximately 12°, stopping short of the 13°54' necessary to become exactly commensurate! Just why this unusual behavior occurs is not understood at this time. The \vec{c}_0^* component remains $\frac{1}{3}c_0^*$, as also reported by Jellinek *et al.*¹⁴ (however, he erred in calling this phase a commensurate phase) and by Williams *et al.*¹⁵ Scruby *et al.*¹⁵ first reported the low-temperature transformation near 200 °K to be to the commensurate $(13)^{1/2}a_0$ and $13c_0$ superlattice (as found in 1T-TaSe₂). Thus

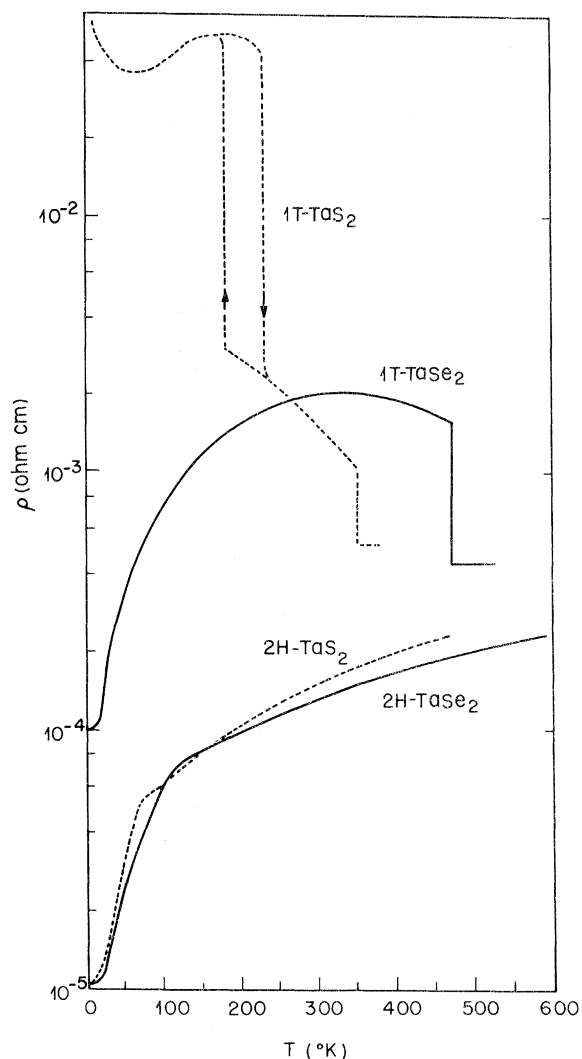


FIG. 1. Electrical resistivity of $1T$ and $2H$ polymorphs of TaS_2 and $TaSe_2$ with the current parallel to the layers ($\rho \perp \vec{c}$). The metal atoms in the $1T$ polymorph are coordinated by an octahedron of chalcogenide atoms, while in the $2H$ polymorph the metal atoms are coordinated by a trigonal prism of chalcogenide atoms. (See Refs. 1 and 2 for details.)

the true lock-in temperature is $T_d \approx 200$ °K, the transition to the "almost" commensurate state at 352 °K we label T'_d . It is not clear why the resistivity at low temperatures (< 200 °K) of the sulfide and selenide are no different, since the same superlattice is reported for both. One can only conjecture that the FS shapes are sufficiently different so that in the case of $1T-TaS_2$, it is almost completely destroyed by gaps in the commensurate state, or that correlations localize the remaining carriers in $1T-TaS_2$.

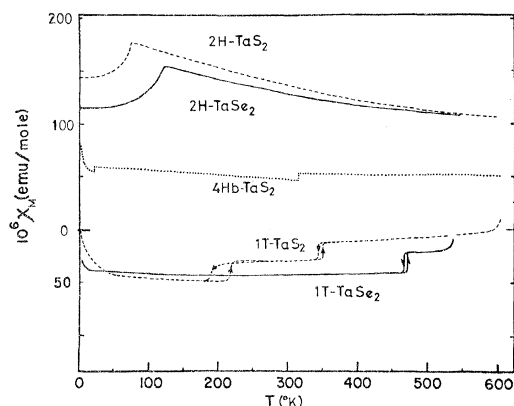


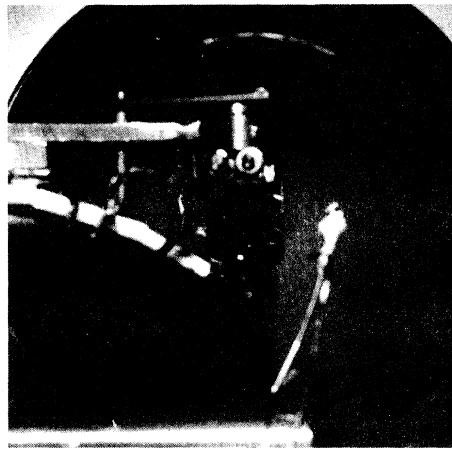
FIG. 2. Magnetic susceptibility (χ) of $1T$ and $2H$ polymorphs of TaS_2 and $TaSe_2$ powders.

We also report here that low-energy-electron-diffraction (LEED) patterns in back reflection show the superlattice in $1T-TaS_2$ and $1T-TaSe_2$, although the resolution is not as good as high-energy-electron-diffraction studies (in transmission).² Figure 3 shows the LEED patterns obtained at room temperature in $2H-TaSe_2$, $1T-TaSe_2$, and $1T-TaS_2$. While $2H-TaSe_2$ shows an undistorted pattern, $1T-TaSe_2$ ($T < T_d$) clearly shows the $(13)^{1/2}$ superlattice. The satellite spots for $1T-TaS_2$ do not fall exactly at the $(13)^{1/2}$ superlattice positions as expected, since for $T_d < T < T'_d$, \vec{q}_0 is not exactly commensurate. This is clearly indicated in Fig. 3(d) by the fact that the satellite spots do not form straight lines as in $1T-TaSe_2$, Fig. 3(c). The small distortions in the $1T-TaSe_2$ pattern are due to small distortions in the electric field. These results show that the CDW extends, unchanged, to the surface of the crystal. Surface effects do not destroy the CDW. Indeed, several authors point out that structural instabilities may be expected to be enhanced at surfaces.^{16, 17}

In both $1T-TaS_2$ and $1T-TaSe_2$, there is considerable information about the incommensurate CDW state and the regimes below T_d . However, little can be learned about T_0 , the onset temperature of the incommensurate CDW, since from electron diffraction we can estimate $T_0 \approx 550$ °K, where conversion of the metastable $1T$ polytype to another ($2H$ or $4H$) polytype occurs. Consequently, information about T_0 is sought from alloy data in the regime of x where the $1T$ structure type is the only stable phase.

B. $1T-Ta_{1-x}Ti_xS_2$

Thompson *et al.* first reported the preparation and properties of $1T-Ta_{1-x}Ti_xS_2$.¹⁸ That study



(a) SAMPLE HOLDER

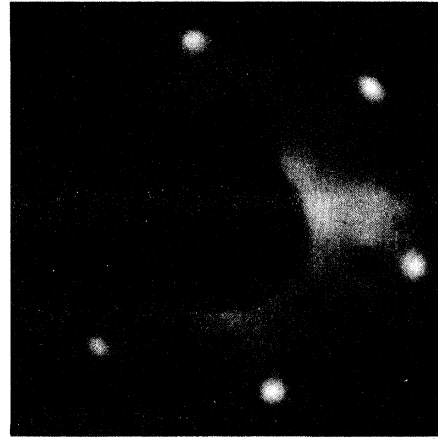
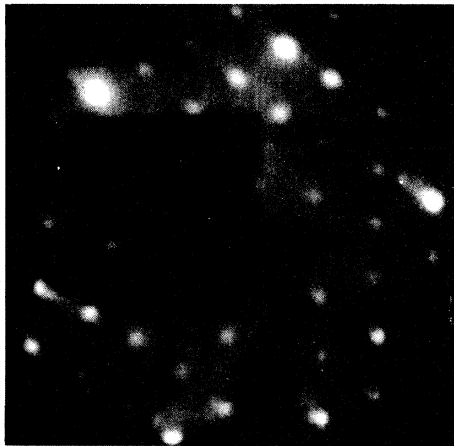
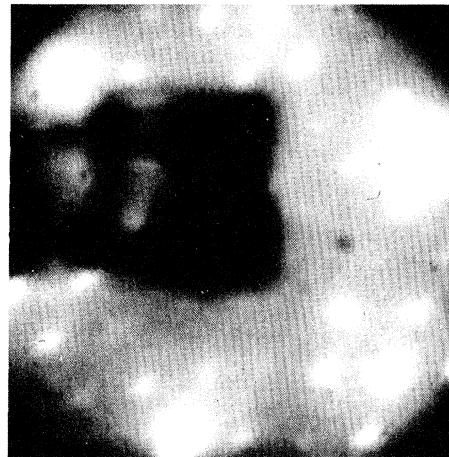
(b) 2H-TaSe₂(c) 1T-TaSe₂(d) 1T-TaS₂

FIG. 3. LEED patterns (300 °K). (a) shows the sample holder in front of the fluorescent screen — the holder obscures the central portion of the diffraction pattern in b–d.

was completed before the cause (i.e., CDW's) of the peculiar properties was understood. The changes in T_d or T'_d could not be followed because studies were performed for x increasing in steps that were too large (multiples of 0.1). Further, no data was obtained in the region near T_0 . However, they pointed out several important features of the system. First, the 1T structure is the only stable polymorph when $x \geq 0.1$. Second, the anomalous behavior of ρ in 1T-TaS₂, specifically its increase at low temperatures, continues

to $x=0.5$. These data prompted us to study this system in more detail.

Electron diffraction studies for $T'_d < T < T_0$ show that as x increased, q'_0 decreased, as expected with a rigid-band model.² Further, these studies show that T_0 is relatively insensitive to increasing x , the effects of the CDW at room temperature are still visible at $x \sim 0.9$. We expect to see, then, the effects of the CDW on the physical properties for a wide range of x .

ρ vs T for several samples with $0 \leq x \leq 0.145$

is shown in Fig. 4. In pure $1T$ - TaS_2 , the resistivity increase at T'_d [$\Delta\rho/\rho(360^\circ\text{K})$] is 1.1 ($\pm 5\%$), and at the 200°K transition ρ increases by a factor of 16. Above T'_d , for at least 25°K , ρ is independent of temperature to 1% at 5×10^{-4} ohm cm. These data for $1T$ - TaS_2 differ somewhat from that presented by Thompson *et al.*¹⁹ in several aspects: the $\Delta\rho$ at T'_d and T_d presented here are larger; we do not find a positive slope to ρ above T'_d , and the hysteresis seen in the low-temperature transformation (40°K) is smaller than observed previously (100°K). These differences are likely due to the fact that the previous samples were not prepared with excess sulfur, the necessity of which was not recognized until more recently.⁷

A number of details concerning Fig. 4 should be pointed out for later use. (i) For this range of x , $\rho(360^\circ\text{K}) \approx 5 \times 10^{-4}$ ohm cm. (ii) As x increases, T'_d decreases, the transition broadening out so that beyond $x \approx 0.15$ no "transition region" is visible. Figure 5 summarizes T'_d vs x data, with the bars representing the approximate transition width. (iii) At low x , $\Delta\rho$ at T'_d at first increases with x , but beyond $x \approx 0.07$ $\Delta\rho$ decreases again. (iv) The 200°K transition is completely suppressed at $x = 0.01$; other samples show this transition is still fully suppressed at $x = 0.005$ and only partial transformation occurs at $x = 0.002$. (v) The resistivity at low temperatures goes through a maximum near $x = 0.085$. This

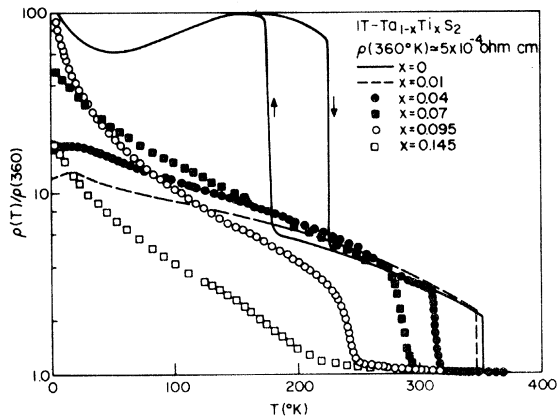


FIG. 4. $\rho \perp \vec{c}$ normalized to $\rho(360^\circ\text{K})$ for $1T - \text{Ta}_{1-x}\text{Ti}_x\text{S}_2$ alloys in the region $0 \leq x \leq 0.15$. The transition at T'_d (the "almost commensurate" transition) showed some hysteresis at the heating or cooling rate of the experiment ($\sim 2^\circ\text{K}/\text{min}$) increasing from 2°K at $x = 0$ to $\approx 10^\circ\text{K}$ at $x = 0.10$. The data shown at T'_d is at the center of the hysteresis loop. The commensurate transition centered at 200°K in $1T - \text{TaS}_2$ is completely suppressed for $x \geq 0.005$.

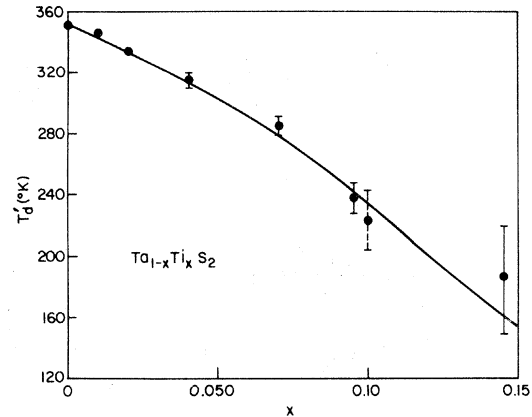


FIG. 5. T'_d vs x for $1T - \text{Ta}_{1-x}\text{Ti}_x\text{S}_2$. The bars represent the approximate transition width from ρ . The point at $x = 0.10$ with a dashed bar is taken from Ref. 18.

is more clearly seen in Fig. 6, where $\rho(4.2^\circ\text{K})/\rho(360^\circ\text{K})$ vs x is shown for a number of samples. The extra data points for alloys with other elements will be discussed later. Figure 7 shows the resistivity for two samples down to 0.5°K . ρ increases approximately as $1/T$ below 20°K when $x = 0.085$. ρ is only slightly affected by magnetic fields; at 0.5°K , for example, when $x = 0$, ρ increases approximately as H^2 so that $\rho(60 \text{ kG}) \approx 2\rho(H = 0)$.

Changes in ρ near T_0 are quite small, as indicated in Fig. 8. ρ is practically constant from T'_d to $\approx 500^\circ\text{K}$, beyond which ρ first decreases

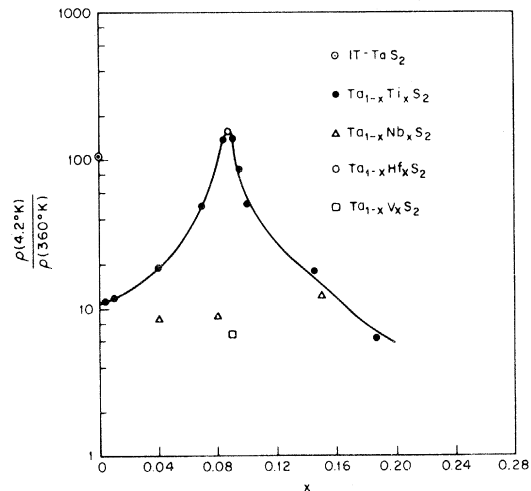


FIG. 6. $\rho(4.2^\circ\text{K})/\rho(360^\circ\text{K})$ for several $1T - \text{TaS}_2$ alloys vs x . For IVb dopants this ratio is ≈ 150 at $x = 0.085$, in contrast to 100 at $x = 0$ or 10 at $x = 0.005$.

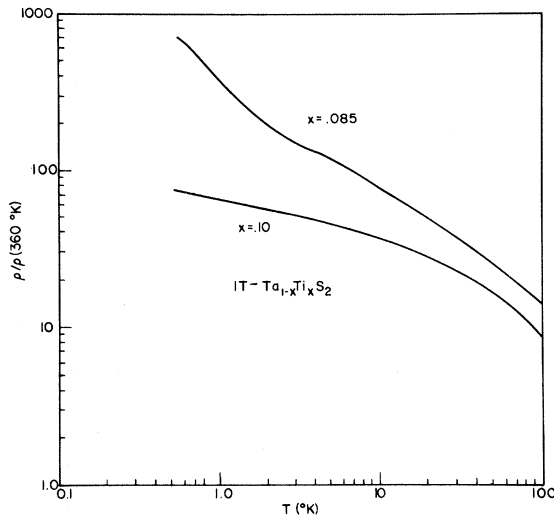


FIG. 7. $\rho \perp \vec{c}$ to 0.5 °K when $x=0.065, 0.10$ for $1T - Ta_{1-x}Ti_xS_2$. At $x=0.085$, ρ increases approximately linearly with $1/T$.

by $\approx 4\%$, and then increases linearly with temperature at $d\rho/dT = 2.7 \times 10^{-9}$ ohm cm/°K. However, the changes are slight, and T_0 cannot be accurately determined from these data.

These changes near T_0 are somewhat more apparent in χ_g , as illustrated in Fig. 9. Above T_0 , χ_g increases linearly with T . If we use the deviation from linearity as a definition of T_0 , we see in Fig. 10, that as x increases T_0 decreases slowly to ≈ 500 °K at $x=0.30$. At $x=0.5$, χ_g does not show a well-defined linear region and T_0 is difficult to estimate (although electron diffraction shows $T_0 > 300$ °K). The χ_g vs T data has been corrected for the effects of 5–10-ppm Fe impuri-

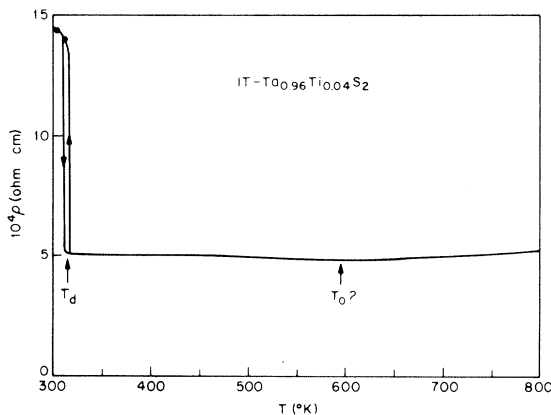


FIG. 8. $\rho \perp \vec{c}$ above 300 °K shows only a weak dip near T_0 . (The charge-density-wave onset temperature.)

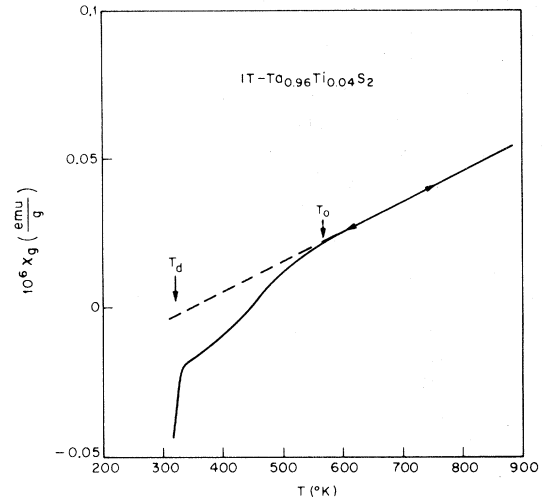


FIG. 9. χ_g of $1T - Ta_{0.96}Ti_{0.04}S_2$ powder above 300 °K shows a dip below T_0 but also continues to increase above T_0 . The arrows on the curve indicate that the results are identical for increasing and decreasing temperature.

ty. This impurity causes the susceptibility at low temperatures to increase as C/T . The total χ below 15 °K varies as $\chi_0 + C/T$, χ_0 and C are constants determined by a fit to the data, and finally C/T subtracted from the measured χ (at all T) to produce Fig. 10. The largest correction to the data is at 4.2 °K and is typically 0.10×10^{-6} emu/g.

When the T_d transformation is suppressed by Ti doping ($0.005 < x < 0.05$), χ_g (4.2 °K) increases by $\approx 0.8 \times 10^{-7}$ emu/g. With a further increase in x , χ_g (4.2 °K) decreases again, reaching a broad minimum near $x=0.1$, after which χ_g (4.2 °K) monotonically increases with x . Note that the minimum in χ_g (4.2 °K) vs x is still considerably above χ_g (4.2 °K) of pure $1T - TaS_2$, even though at 4.2 °K $\rho(x=0.085) > \rho(1T - TaS_2)$. The χ_g of a sample at $x=0.085$ [χ_g (4.2 °K) $\approx -0.125 \times 10^{-6}$ emu/g] is similar to that at $x=0.15$.

The results of DSC measurements are shown in Fig. 11. The enthalpy of transition of $1T - TaS_2$ at T_d (200 °K) is 18 cal/mole,¹⁹ a factor of 7 smaller than ΔH at T'_d ($\Delta H'_d$). Most of the commensurability energy (ΔH) is obtained at T'_d , as would be expected from the sensitivity of the transition at T_d to very small doping. The transition width increases with increasing x , as also observed in ρ measurements. Consequently, the estimated accuracy of the measurement decreases with increasing x , as shown by the "error bars." At 8-at.% Ti, no transition could be detected above the noise, probably due to the larger transition width. The enthalpy of transition $\Delta H'_d$ initially increases with x , a plateau occurring in the range $0.02 < x < 0.06$.

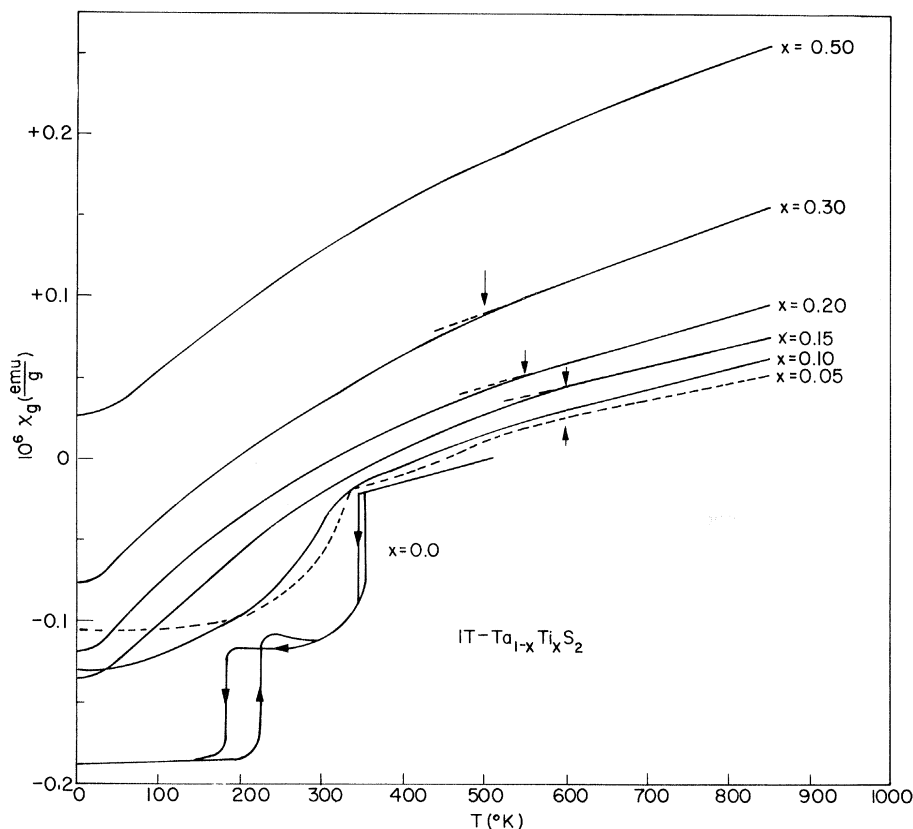


FIG. 10. χ_g of $1T$ $-\text{Ta}_{1-x}\text{Ti}_x\text{S}_2$ powders from 4.2 to $\approx 900^\circ\text{K}$, indicating the decrease in T_0 with increasing x . The data have been corrected at low temperatures for a small impurity contribution proportional to $1/T$. (Arrows mark T_0 .)

Note in this system that *both* ΔH and $\Delta\rho$ initially increase with increasing x . Since data was not obtained in this system for $x > 0.06$, it is difficult to estimate where $\Delta H \rightarrow 0$.

The ρ data suggest that for $x \geq 0.005$, the CDW remains incommensurate to $T=0$. The reduction in conduction electron density (electrons per atom, \bar{z}) and/or cation disorder eliminates T'_d at very small x , and reduces T'_d at $10^\circ\text{K}/\text{at}\%$ Ti, but does not have much effect on T_0 . The large ρ obtained for $x \approx 0.085$ and the initial increase in ΔH and $\Delta\rho$ at T'_d vs x may be due to a changing \bar{z} or possibly disorder. In all of the above changes, it is not immediately clear whether \bar{z} or disorder—or some combination—is responsible for the change. The following data on other $1T$ -alloy systems will help settle this question and allow us to formulate a picture of the effects of doping on the CDW, particularly on T'_d and T_d .

C. $1T\text{-Ta}_{1-x}\text{Nb}_x\text{S}_2$ and $1T\text{-Ta}_{1-x}\text{V}_x\text{S}_2$

In these alloys \bar{z} is constant, since all the cations are from the same column of the periodic table. The effects on the CDW of doping should be primarily due to cation disorder. Some small

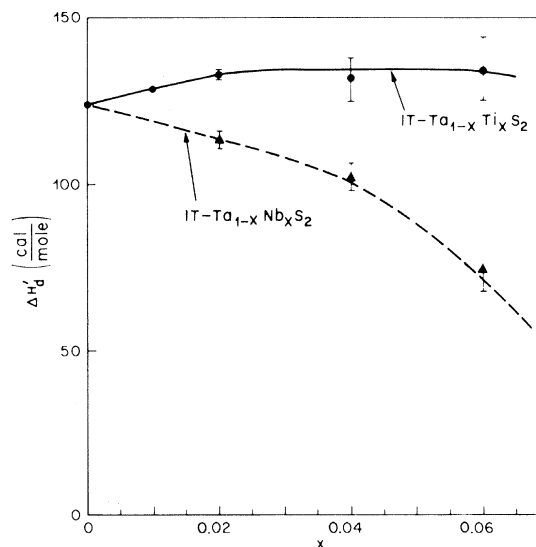


FIG. 11. Enthalpy of transformation, $\Delta H'_d$ at T'_d in Ti- and Nb-doped $1T - \text{TaS}_2$ by differential-scanning-calorimetry (DSC). The thermal anomaly at T'_d at heating or cooling rates of $10^\circ\text{K}/\text{min}$ is broader than that seen in ρ (Fig. 4) except at $x=0$. At $x=0.06$ the thermal anomaly was $\approx 30^\circ\text{K}$ wide, making exact calculation of $\Delta H'_d$ less reliable. By $x=0.085$ the anomaly was either too wide or $\Delta H'_d$ too small to be seen above the noise level of the instrument.

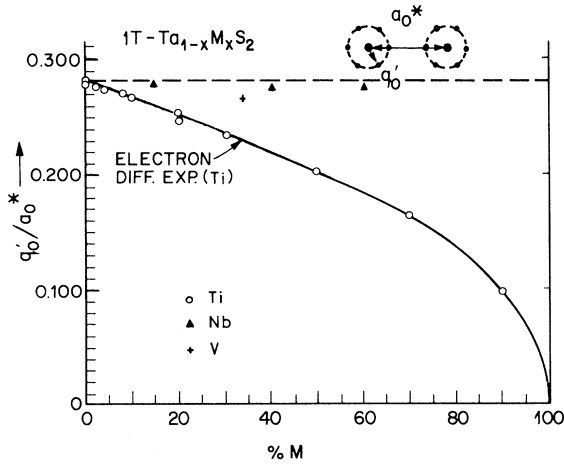


FIG. 12. $|\vec{q}_0^*|/|\vec{a}_0^*|$ vs x for Ti, V, Nb alloys of $1T - \text{TaS}_2$ when $T > T'_d$ (from Ref. 2). q_0^* is the basal plane [i.e., $(hk0)$] projection of the CDW distortion wave vector, and in the rigid-band approximation, should decrease with increasing Ti content but remain almost constant for V and Nb.

changes in the band structure might be expected, however, because of the difference in radial extent of $3d-4d-5d$ wave functions.

In Fig. 12 we show the results of electron-diffraction measurements in $1T - \text{Ta}_{1-x}M_x\text{S}_2$ for $M = \text{Ti}$, Nb, or V at $T > T'$, as taken from Ref. 2. While $|\vec{q}_0^*|/|\vec{a}_0^*|$ decreases with x for $M = \text{Ti}$, it is constant for $M = \text{Nb}$ and almost so for V. These results are expected, since \vec{q}_0^* should be the spanning vector of the average rigid band of the alloy series.

ρ vs T and χ vs T for $1T - \text{Ta}_{1-x}\text{Nb}_x\text{S}_2$ are shown in Figs. 13 and 14, respectively. T'_d is suppressed at about the same rate as in the $\text{Ta}_{1-x}\text{Ti}_x\text{S}_2$ series, although the size of the resistive anomaly is decreased quickly with Nb addition. Again, the transition at T_d is fully suppressed at small doping. We note further that $\rho(4.2 \text{ K})/\rho(360 \text{ K}) \approx 10$ and independent of x , even up to $x = 0.6$. This is in marked contrast to the $\text{Ta}_{1-x}\text{Ti}_x\text{S}_2$ series. Figure 14 shows that even at $x = 0.6$, χ_g decreases to quite low values at low T , again in contrast to the behavior of the $\text{Ta}_{1-x}\text{Ti}_x\text{S}_2$ series at large x .

The results of DSC measurements on the Nb-doped samples is shown in Fig. 11, in comparison to the Ti-doped samples. $\Delta H'_d$ decreases as x increases. If the curve is extended, we estimate $\Delta H'_d \rightarrow 0$ when $0.08 < x < 0.10$, approximately where $\Delta\rho \rightarrow 0$.

ρ was measured for only two compositions of $1T - \text{Ta}_{1-x}\text{V}_x\text{S}_2$, as shown in Fig. 15. The increase in ρ at low temperatures is smaller than

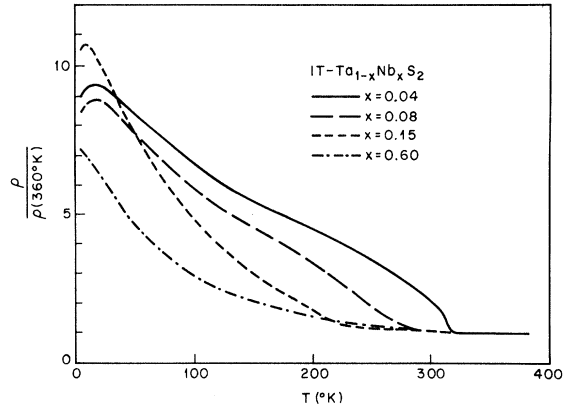


FIG. 13. $\rho \perp \vec{c}$ for $1T - \text{Ta}_{1-x}\text{Nb}_x\text{S}_2$ alloys. The elimination of the commensurate transition at T_d and the rapid suppression of the almost commensurate transition at T'_d , similar to the $1T - \text{Ta}_{1-x}\text{Ti}_x\text{S}_2$ alloys, shows that cation disorder is primarily responsible for these changes, not changes in conduction-electron density (β).

expected in light of the Nb results, but the elimination of T_d and suppression of T'_d is quite evident.

These measurements show that the elimination of T_d and decrease of T'_d by cation doping in $1T - \text{TaS}_2$ is due primarily to cation disorder. While cation disorder alone decreases $\Delta H'_d$, if β is decreased $|\vec{q}_0^*|$ decreases toward its commensurate value, which should be attained near $x = 0.025$. This apparently increases $\Delta H'_d$ by approximately 20 cal/mole, as estimated from Fig. 11. It would also appear that the large increase in ρ at low T in Ti-doped samples near $x \approx 0.085$ is due to changes in β .

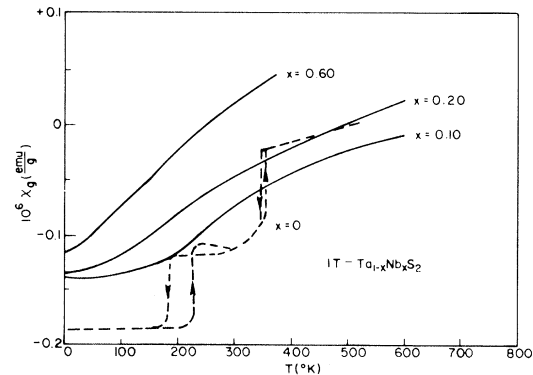


FIG. 14. χ_g of $1T - \text{Ta}_{1-x}\text{Nb}_x\text{S}_2$ powders, corrected at low T for a small paramagnetic impurity contribution proportional to $1/T$. These alloys remain quite diamagnetic at low T , in contrast to $1T - \text{Ta}_{1-x}\text{Ti}_x\text{S}_2$ alloys (Fig. 10).

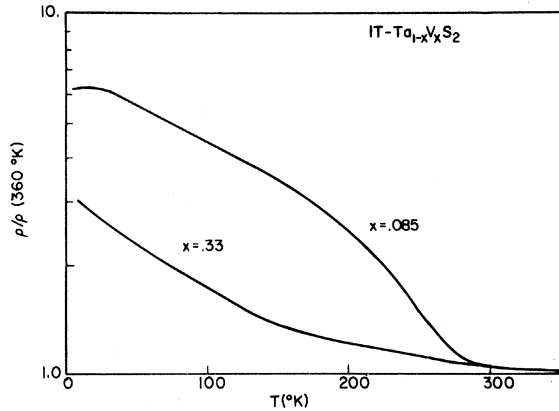


FIG. 15. $\rho \perp \vec{c}$ for $1T - \text{Ta}_{1-x}\text{V}_x\text{S}_2$ alloys, again shows rapid suppression of transitions at T'_d and T_d are a cation-disorder effect.

D. $1T - \text{Ta}_{1-x}\text{Zr}_x\text{S}_2$ and $1T - \text{Ta}_{1-x}\text{Hf}_x\text{S}_2$

If the large increase in ρ at low temperatures of $1T - \text{Ta}_{0.915}\text{Ti}_{0.085}\text{S}_2$ is due to a low-conduction-electron density in the CDW state, then similar changes ought to be observed in these two systems. Previous electrical measurements on $1T - \text{Ta}_{0.85}\text{Zr}_{0.15}\text{S}_2$ showed $\rho(4.2^\circ\text{K})/\rho(300^\circ\text{K}) \approx 20$.²⁰ Figure 16 compares ρ for $1T - \text{Ta}_{0.915}\text{Hf}_{0.085}\text{S}_2$ and $1T - \text{Ta}_{0.915}\text{Ti}_{0.085}\text{S}_2$ [see also Fig. 6 for $\rho(4.2^\circ\text{K})/\rho(360^\circ\text{K})$]. Note that the shape of this curve is quite different from that of $1T - \text{Ta}_{0.915}\text{Ti}_{0.085}\text{S}_2$ especially in the region near T'_d . No evidence for a transition near T'_d is seen in the Hf sample—indicating that T'_d is more rapidly suppressed with Hf doping. The high ρ at 4.2°K is observed in both systems, even though the Ti-doped sample shows a transition at T'_d and that transition is fully suppressed in the Hf sample. Although the transition at T'_d should increase the amplitude of the CDW and thus decrease the carrier density by larger FS gaps (removing more FS—as reflected by the jump in ρ at T'_d), this apparently has little effect on ρ at temperatures much below T'_d . This would suggest that the transition at T'_d is a small perturbation on the CDW, at least when $x=0.085$. $\Delta H'_d$ at this x may be quite small, so this conclusion cannot necessarily be carried through to the pure materials.

The Hall constant R_H was also measured for this Hf-doped sample to 90°K ; below this temperature difficulties were encountered due to the small value of R_H and the rapidly increasing value of ρ . At $T=300^\circ\text{K}$, $R_H = -2.9 \times 10^{-4} \text{ cm}^3/\text{C}$, leading to a Hall mobility μ_H of $0.5 \text{ cm}^2/\text{V sec}$. As T decreases R_H increases, but not as rapidly as ρ . Thus at 90°K $R_H = -9 \times 10^{-4} \text{ cm}^3/\text{C}$ and

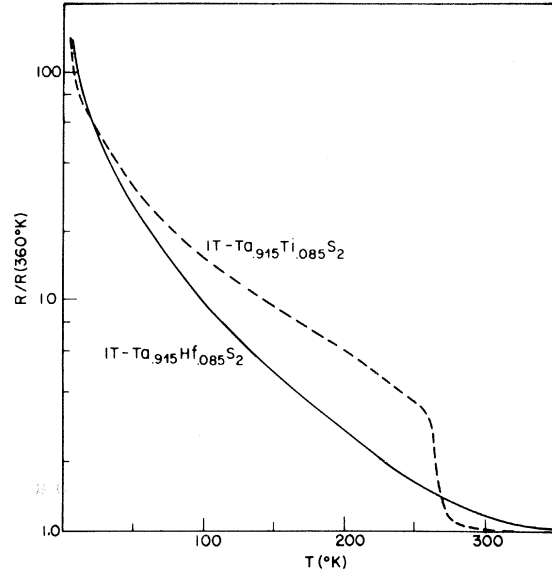


FIG. 16. $\rho \perp \vec{c}$ at $x=0.085$ for Ti- and Hf-doped $1T - \text{TaS}_2$. While the rate of suppression of the almost commensurate transition at T'_d depends upon the dopant cation, the resistivity at low temperatures depends more on E .

$\mu_H = 0.13 \text{ cm}^2/\text{V sec}$. These values are difficult to interpret, however, due to the probable presence of both hole and electronlike carriers. In comparison, the values obtained for $2H - \text{NbSe}_2$ in this region are $R_H = 4.9 \times 10^{-4} \text{ cm}^3/\text{C}$ and $\mu_H = 3 \text{ cm}^2/\text{V sec}$, as previously observed.^{21,22}

The thermopower S of the same Hf-doped sample was measured, vs high-purity Cu, and is shown in Fig. 17. Although R_H indicates a pre-

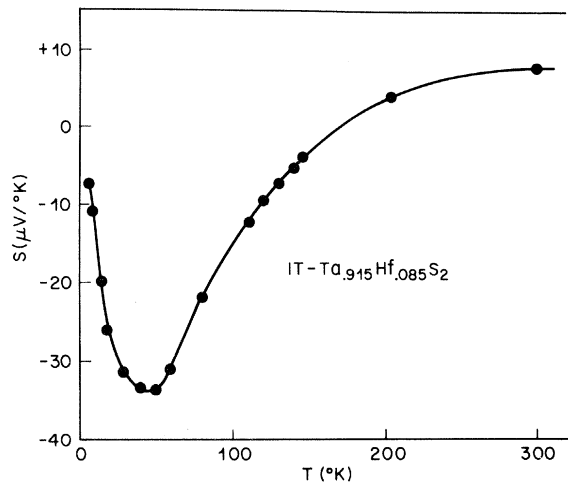


FIG. 17. The thermopower of $1T - \text{Ta}_{0.915}\text{Hf}_{0.085}\text{S}_2$ from 4.2 to 300°K measured vs high-purity Cu.

dominance of electronlike carriers, S reverses sign near 170 °K. The small positive thermopower of pure Cu (less than $1.5 \mu\text{V}/^\circ\text{K}$ below 300 °K)²³ has not been subtracted out, since it shifts this curve by only a very small amount. While S must go to zero as $T \rightarrow 0$, the maximum value obtained is $-34 \mu\text{V}/^\circ\text{K}$ at 45 °K. Again this can be compared to $2H\text{-NbSe}_2$, where S_H also reverses sign at low temperatures, but at low temperatures is less than $5 \mu\text{V}/^\circ\text{K}$.^{21, 22} Interpretation of these data is again difficult, especially since S can be changed by doping in metal systems and can become large in transition metals themselves ($\approx 30 \mu\text{V}/^\circ\text{K}$).²³

Although it would clearly be desirable to obtain further R_H measurements in these systems, it is clear that the increase in ρ at low temperatures for group-IVb dopants near $x=0.085$ is due to a decreasing β .

E. $1T\text{-Ta}_{1-x}\text{Ti}_x\text{Se}_2$ and $1T\text{-Ta}_{1-x}\text{Zr}_x\text{Se}_2$

In $1T\text{-Ta}_{1-x}\text{M}_x\text{S}_2$ the commensurate transition at T_d is eliminated for x greater than 0.002, but the "almost commensurate" transition at T'_d is little affected. Since in $1T\text{-TaSe}_2$ there is no T'_d transition, it is of interest to determine the effect of doping on T_d in $1T\text{-TaSe}_2$.

$\rho/\rho(500^\circ\text{K})$ vs T is shown for x up to 0.15 in Fig. 18 for $1T\text{-Ta}_{1-x}\text{Ti}_x\text{Se}_2$. Here we see that T_d is not rapidly eliminated as in the corresponding sulfide but is suppressed at a rate ($\approx 13^\circ\text{K}/\text{at.}\%$ Ti) similar to that of T'_d in the sulfide ($\approx 10^\circ\text{K}/\text{at.}\%$ Ti), but $\Delta\rho$ at T_d decreases with

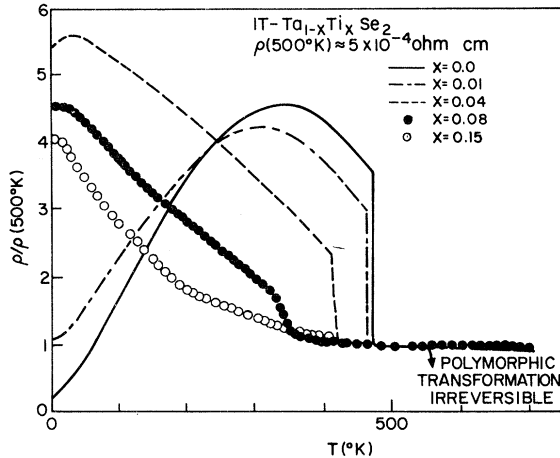


FIG. 18. $\rho \perp \vec{c}$ for $1T\text{-Ta}_{1-x}\text{Ti}_x\text{Se}_2$ vs T . $1T\text{-TaSe}_2$ does not show an almost commensurate transition. The entire lock-in enthalpy ΔH_d is obtained at T_d . The suppression of T_d with increasing x ($\approx 13^\circ\text{K}/\text{at.}\%$ Ti) is similar to the suppression of T'_d in $1T\text{-Ta}_{1-x}\text{Ti}_x\text{S}_2$ (see Fig. 5).

x , in contrast to the sulfide at T'_d . A comparison of these results to those of $1T\text{-Ta}_{1-x}\text{Ti}_x\text{S}_2$ shows that the T'_d transition in the sulfide is much like T_d in the selenide. This is not surprising, since in the sulfide most of the commensurability energy is obtained at T'_d .

The magnetic susceptibility of $1T\text{-Ta}_{0.9}\text{Ti}_{0.1}\text{Se}_2$ above room temperature is shown in Fig. 19. T_0 is not as easily seen here as in the corresponding sulfide (see Fig. 10)—note only the slight dip in χ near 600 °K. Also, the susceptibility at high temperatures does not become as large as in the sulfide (see Fig. 10—even on a per mole basis).

DSC measurements show that ΔH_d decreases at T_d for increasing x (Fig. 20). Again the transition broadened with increasing x so that an anomaly could not be detected at $x=0.08$. A linear extrapolation would estimate $\Delta H \rightarrow 0$ at $x \approx 0.10$, in rough agreement with the point at which $\Delta\rho \rightarrow 0$. It would appear that beyond $x=0.10$, the CDW remains incommensurate at $T=0$.

$1T\text{-Ta}_{1-x}\text{Zr}_x\text{Se}_2$ compounds are very similar to the corresponding Ti compound, but T_d decreases somewhat faster ($\approx 18^\circ\text{K}/\text{at.}\%$) as does ΔH_d (see Fig. 20). In this alloy series we estimate $\Delta H_d \rightarrow 0$ at $x \approx 0.08$, and the CDW should remain incommensurate at all T for $x > 0.08$.

F. $1T\text{-Nb}_{1-x}\text{Ti}_x\text{Se}_2$

$1T\text{-Nb}_{0.5}\text{Ti}_{0.5}\text{Se}_2$ has been reported²⁰ but showed no evidence of a commensurate-incommensurate transition. Such a transition appears if the Ti concentration is reduced below $\approx 10\%$, if the $1T$ phase is retained at room temperature. Electron-

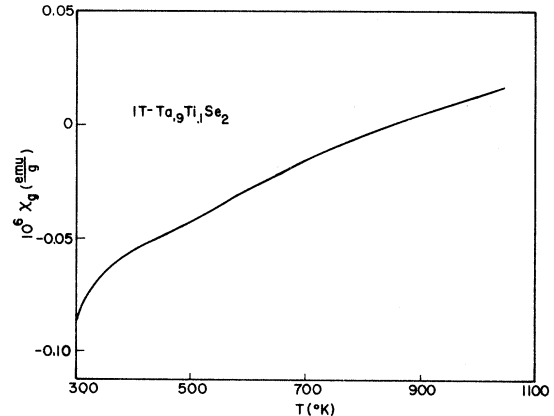


FIG. 19. χ_g of $1T\text{-Ta}_{0.9}\text{Ti}_{0.1}\text{Se}_2$ powder above 300 °K. The slight dip occurring near 600 °K may be indicative of the CDW onset T_0 .

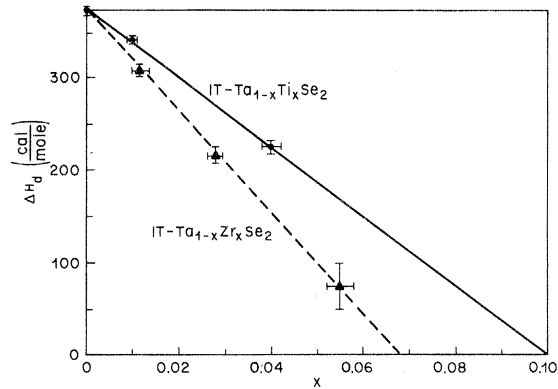


FIG. 20 Enthalpy of transformation ΔH_d at T_d in Ti- and Zr-doped $1T-\text{TaSe}_2$. Again due to decreasing ΔH_d and increasing transition widths, no data was obtained beyond $x=0.06$. The bars represent the estimated errors in determining x and ΔH_d .

diffraction patterns from these compounds were similar to those obtained from the corresponding Ta compound (when $T > T_d$). ρ of $1T-\text{Nb}_{0.94}\text{Ti}_{0.06}\text{Se}_2$ (Fig. 21) shows evidence for T_d at $\approx 335^\circ\text{K}$. At higher x , T_d appears to be rapidly suppressed. The $1T$ phase could not be retained for $x < 0.06$. If we estimate dT_d/dx as $\approx 15^\circ\text{K/at.}\%$, T_d of pure $1T-\text{NbSe}_2$ (if it could be retained at room temperature) would be $\approx 425^\circ\text{K}$. Although it would have been interesting to compare these results to those obtained on $1T-\text{Nb}_{1-x}\text{Zr}_x\text{Se}_2$, we found that Zr is not soluble in NbSe_2 at levels greater than $\approx 0.5\%$, and the $1T$ polymorph could not be prepared.

G. Other cation-doped compounds

We have prepared alloys $1T-\text{Nb}_{1-x}\text{Ti}_x\text{S}_2$ for $x \geq 0.04$. At $x=0.04$, electron diffraction indicates a transition from incommensurate $(\vec{q}_0^* \approx 0.270 \vec{a}_0^*)$, very close to that for $1T-\text{Ta}_{0.96}\text{Ti}_{0.04}\text{S}_2$, see Fig. 12) to a commensurate $(13)^{1/2} \vec{a}_0^*$ superlattice (of the $1T-\text{TaSe}_2$ type) at $\approx 320^\circ\text{K}$. Thus $1T-\text{NbS}_2$, if it could be prepared, will not likely show the intermediate "almost commensurate" state of $1T-\text{TaS}_2$. We also find that Zr is not very soluble in NbS_2 and were unable to produce $1T-\text{Nb}_{1-x}\text{Zr}_x\text{S}_2$ similar to our findings for NbSe_2 .

We have attempted to produce $1T-\text{Ta}_{1-x}\text{W}_x\text{S}_2$ but find that W is included only to $x \approx 0.01$. At this point T_d' is suppressed to $\approx 335^\circ\text{K}$, and the resistive anomaly is small and considerably broadened. It appears that higher W content is not obtained because the transport rate of W during crystal growth with iodine is much smaller than that of Ta. We are attempting to prepare

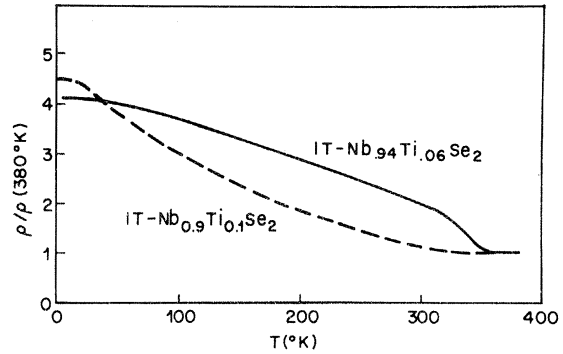


FIG. 21. $\rho \perp \vec{c}$ of $1T-\text{Nb}_{1-x}\text{Ti}_x\text{Se}_2$. Although $1T-\text{NbSe}_2$ could not be prepared, we can estimate from this data, using dT_d/dx as $15^\circ\text{K/at.}\%$, that $T_d \approx 425^\circ\text{K}$ for pure $1T-\text{NbSe}_2$.

crystals at higher x by using different chemical-transport agents.

H. $1T-\text{TaS}_{2-x}\text{Se}_x$

The influence of anion disorder on T_d and on the formation of the "almost commensurate" state in $1T-\text{TaS}_2$ can be studied in this alloy system. While the number of conduction electrons per cation remains constant in this series, some changes in the Fermi surface should occur due to different cation-anion mixing. Some differences in the FS as calculated by the Korringa-Kohn-Rostoker (KKR) method have been given by Myron and Freeman.²⁴

ρ for a series of these alloys is presented in Figs. 22 and 23. These results differ sharply from those of the cation alloys. The first-order transition at T_d' remains quite sharp and increases smoothly from 352°K at $x=0$ to 473°K at $x=2$, as shown in Fig. 24. The low-temperature transformation to the commensurate state at T_d characteristic of $1T-\text{TaS}_2$ extends to $x=0.8$, although at this temperature it is so sluggish that it only partially occurred upon warming the sample. Note also the high resistivity at 4.2°K of those samples showing the low-temperature transformation. A sample at $x=1$ was slowly cycled between 80 and 200°K for 6 h, but no evidence of transformation was seen.

The enthalpy of transformation ΔH at the higher transition (T_d') as observed by DSC is shown also in Fig. 24. The enthalpy of transformation was reproducible on a given sample to $\pm 2\%$ and was determined by comparison to the enthalpy of melting of In (although the reported ΔH values of In, a melting standard, vary by $\pm 3\%$, we use 6.8 cal/mg). The values obtained for $1T-\text{TaS}_2$ and

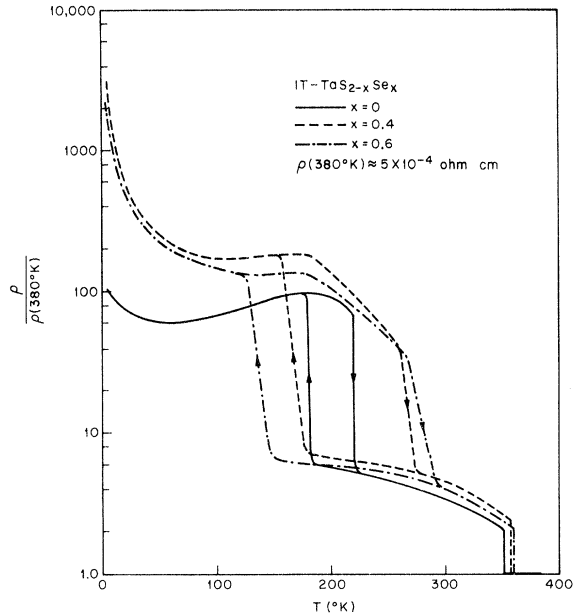


FIG. 22. $\rho \perp \vec{c}$ normalized to $\rho(380^\circ\text{K})$ of $1T-\text{TaS}_{2-x}\text{Se}_x$ for $0 \leq x \leq 0.6$. Since ρ above T_d is approximately temperature independent for $\approx 100^\circ\text{K}$, we normalize to $\rho = 5.0 \times 10^{-4}$ ohm cm somewhat above T_d for $x = 0.6$.

$1T-\text{TaSe}_2$ are 123 and 374 cal/mole, respectively. The latter value for $1T-\text{TaSe}_2$ is 10% larger than we previously reported⁸—the earlier value being incorrect due to a miscalibration of the apparatus.

Electron diffraction at room temperature shows the satellite spots to be similar to those² seen in $1T-\text{TaS}_2$ up to $x \approx 0.8$, except that the spots have become more diffuse, those that were very close (in little triangular clusters) merging into a larger "blob." For $x \geq 1.0$ the patterns are very similar to $1T-\text{TaSe}_2$.

It appears that the "almost commensurate" regime of $1T-\text{TaS}_2$ is not fully suppressed until $x \approx 1.0$, and that for $x \geq 1.0$ the transition is to the fully commensurate state observed in $1T-\text{TaSe}_2$. Considerable anion disorder does not inhibit the T_d transition in $1T-\text{TaS}_2$, nor does it broaden the transition at T'_d (in contrast to the effects of cation doping). On the other hand, when $x \geq 1$, anion disorder does reduce ΔH_d —the commensurability enthalpy—from that of $1T-\text{TaSe}_2$.

V. DISCUSSION

From these data, a consistent picture of the effects of doping on the CDW can be developed. In those pure materials studied, the incommensurate CDW state becomes stable below an onset temperature T_0 . At T_d ($T_d < T_0$), a first-order transition to the commensurate state occurs,

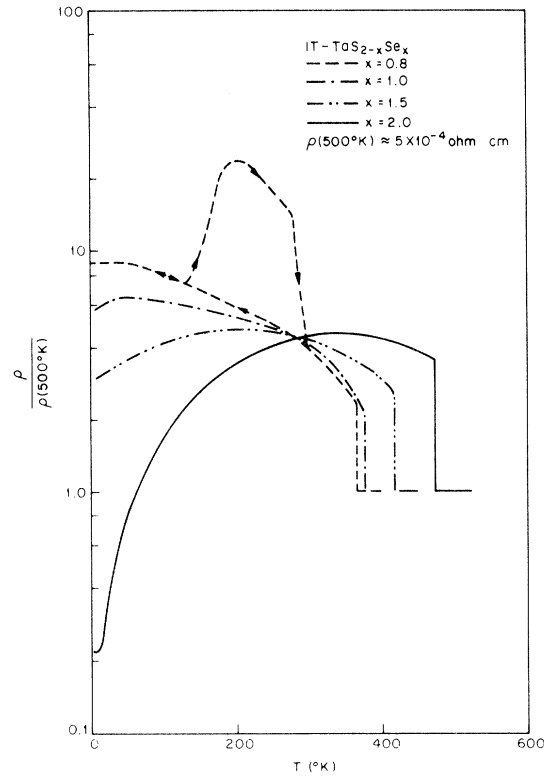


FIG. 23. $\rho \perp \vec{c}$ normalized to $\rho(500^\circ\text{K})$ of $1T-\text{TaS}_{2-x}\text{Se}_x$ for $0.6 \leq x \leq 2.0$, again $\rho(500^\circ\text{K}) \approx 5 \times 10^{-4}$ ohm cm.

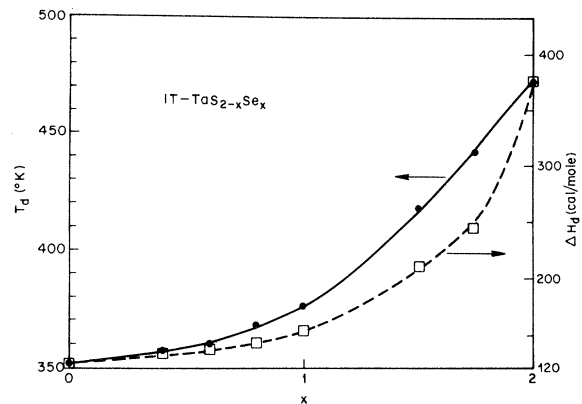


FIG. 24. T_d and ΔH_d vs x for $1T-\text{TaS}_{2-x}\text{Se}_x$ single crystals. Note for $x < 1.0$, the transition is to the "almost commensurate" state; thus we should use T'_d and $\Delta H'_d$. Anion disorder does not affect the transition at T_d (or T'_d) in a serious way, as does cation disorder. We see, however, that T_d and ΔH_d are reduced below a straight-line extrapolation between $1T-\text{TaS}_2$ and $1T-\text{TaSe}_2$ values.

which remains stable to $T=0$. In $1T$ -TaS₂ an intermediate state occurs below T_0 at T'_d ($T_d < T'_d < T_0$) in a first-order transition. This state is "almost commensurate." Most of the enthalpy of transformation occurs at T'_d , and indeed it is T'_d that responds much like the commensurate transition in $1T$ -TaSe₂ (vs doping). The $1T$ -TaS₂ transition at T_d is lost at very small doping levels on the order of 0.2% or less. Thus it appears that $1T$ -TaS₂ with this small doping remains incommensurate to $T=0$. The sensitivity of T_d to impurities (and presumably to nonstoichiometry) probably explains the absence of this transition in some nominally pure $1T$ -TaS₂ samples.^{25, 26}

Doping with cations reduces T_d (or T'_d) and broadens the transition; in $1T$ -TaSe₂ the commensurate state is fully suppressed when $x \approx 0.10$ (for the cations studied here). When the first-order transition ceases to occur ($\Delta H_d = 0$), T_d or T'_d has *not* decreased to zero; the transition just "fades out." The random-cation potential rapidly destroys the electrostatic energy gained by lock-in. Since one of the cations is more electropositive than the other, the charge maxima centered on these cations at lock-in would prefer to be on the more electronegative cation. This reduces the energy gained at lock-in, and at large enough doping, only the incommensurate state can exist. Consistent with this picture, the data show that as the electronegativity difference between the dopant cation and host cation is increased, dT_d/dx becomes larger and the incommensurate phase is stabilized at $T=0$ for lower x . This observation is consistent with a recent proposal that electronegativity has an important role in the transition at T_d (or T'_d) of the *pure* layered compounds showing CDW behavior.²⁷

Anion disorder, at least in TaS_{2-x}Se_x, does not suppress the lock-in transitions, and they remain sharp for all x . This suggests that those conduction electron states at the FS involved in CDW formation have little or no anion s or p character mixed in. The data suggest that for $x \geq 1$, where only one transition is seen, it is to a commensurate superlattice state similar to that of $1T$ -TaSe₂. This, however, should be confirmed by neutron or x-ray scattering.

The properties near T_0 can only be studied with group IVb dopants when $x \geq 0.05$, in order that the $1T$ phase remain stable. Only very small effects in ρ and somewhat larger effects in χ are observed near T_0 . No change in heat capacity was observed in this region, it presumably being too small to see or to spread out due to the effects of the dopant. T_0 decreases slowly with increasing x by ≈ 100 °K when x is 0.3. The magnetic sus-

ceptibility in $1T$ -Ta_{1-x}Ti_xS₂ reaches quite large values for $T \approx T_0$ (compare to $2H$ -TaS₂ in Fig. 2). This is unexpected, since the calculated density of states of $1T$ -TaS₂ is smaller than that of $2H$ -TaS₂. Further, χ continues to increase for $T > T_0$, suggesting large temperature-dependent enhancements of the $q=0$ susceptibility. Again, neutron-diffraction studies would help our understanding of the onset of the CDW. Such studies could also determine the nature of the diffuse scattering observed in the region $T_d < T < T_0$.² While we believe that this scattering is probably due to transverse CDW excitations (Overhauser calls them phasons), others have ascribed it to Kohn anomalies in the parent FS.¹⁵ But the latter is not likely to be the case below T_0 , since the FS is already distorted; neutron studies should resolve the question. More careful studies of the heat capacity near T_0 , particularly differential measurements on large samples, are necessary to determine the thermal properties near T_0 . These measurements would determine the free energy of the CDW state relative to the normal state.

With group IVb dopants, the resistivity rises to near 10^{-1} ohm cm at 4.2 °K when $x \approx 0.085$. This is clearly related to the δ produced by the doping; but since ρ increases approximately as T^{-1} at low T , it does not appear to be due to a simple loss of carriers excited across a FS gap. Measurements on one compound ($1T$ -Ta_{0.915}Hf_{0.085}S₂) suggest a decrease in mobility, as well as carrier concentration with decreasing temperature. Relatively large ρ at 4.2 °K are also observed in $1T$ -TaS₂ and several $1T$ -TaS_{2-x}Se_x alloys. Since ρ again increases approximately as T^{-1} at low T (at least in the anion alloys), it appears that in the commensurate state (below T_d) δ is again small enough to produce the effects seen in the IVb-doped alloys. It seems possible that at the proper value of δ , the incommensurate CDW or the commensurate superlattice reduces the effective carrier density to a point where screening is considerably reduced and the remaining electrons become trapped losing their mobility. In *all* the alloys, even away from $x = 0.085$, ρ increases at low T , perhaps due to enhanced scattering from the impurities as the amplitude of the CDW increases.

The CDW is known to be affected also by intercalation (e.g., ethylene diamine in $1T$ -TaS₂, see Ref. 2), but studies here are less complete. Although we have not discussed the CDW in $2H$ polytypes here, it is known that intercalation and cation (or anion) disorder effect the CDW formation and superconducting properties of $2H$ -TaS₂.²⁸

These results for the $1T$ alloys are consistent

with a free-energy model recently proposed by W. L. McMillan.²⁹ If the model is expanded to include a coupling to secondary distortions and a consequent variation of the \tilde{q}_i with temperature, as observed and proposed in a free-energy model for $2H$ -TaSe₂ by D. E. Moncton *et al.*,³⁰ and to include an explicit coupling of free carriers to CDW excitations, it is hoped that all of the effects observed in these systems can be understood—at least by a “macroscopic” Landau-type model. The data presented here will allow an estimation of various parameters in the theory, particularly those that determine the lock-in at T_d and the interaction of the CDW with a random-impurity potential. It is not yet clear whether the model can predict “almost commensurate” transitions, as seen in $1T$ -TaS₂ and some of its alloys.

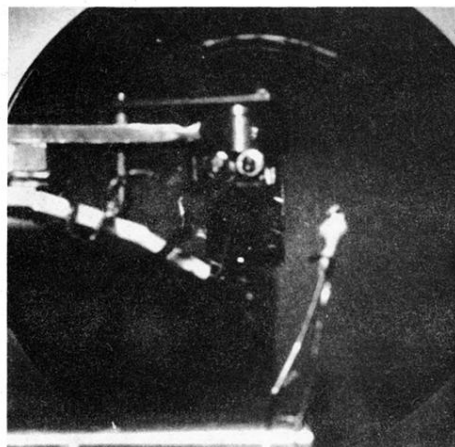
Future work will include studies of more electro-negative dopants in $1T$ structures and a search for other CDW systems. Work in progress includes neutron-scattering and optical studies. Other work will include improved studies of R_H , S , and a de Haas-van Alphen determination

of the FS in normal and CDW layered compounds. Our work and that of several other groups on both experimental and theoretical fronts should lead to a more detailed understanding of the CDW state, at least in these systems, and hopefully will lead to a larger understanding of instabilities in metals.

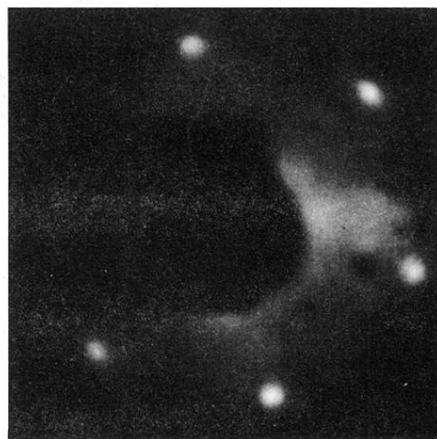
ACKNOWLEDGMENTS

The electron diffraction studies reported here were done in collaboration with S. Mahajan and are greatly appreciated. We would like to thank G. W. Hull, Jr. for measuring ρ of several samples to 0.5 °K and the thermopower measurement, and also C. W. Caldwell, Jr. for the LEED measurements on the pure layered compounds. Continuing discussions with S. Mahajan and D. E. Moncton concerning CDW systems have been very helpful. We would also like to thank A. H. Thompson and B. G. Silbernagel for discussing their results, and W. L. McMillan for enlightening discussions and preprints of his Landau calculations on CDW formation in layered compounds.

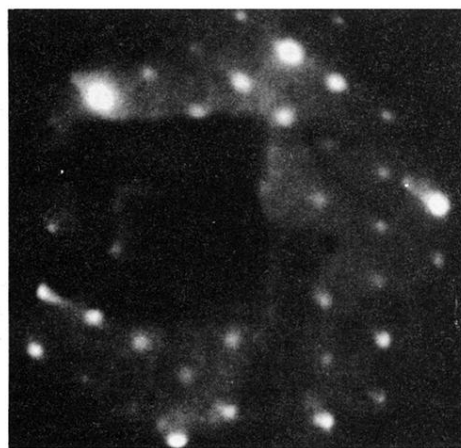
-
- ¹J. A. Wilson, F. J. Di Salvo, and S. Mahajan, *Phys. Rev. Lett.* **32**, 882 (1974).
²J. A. Wilson, F. J. Di Salvo, and S. Mahajan, *Adv. in Phys.* **24**, 117 (1975).
³J. A. Wilson and A. D. Yoffe, *Adv. in Phys.* **18**, 193 (1969).
⁴L. F. Mattheiss, *Phys. Rev. B* **8**, 3719 (1973).
⁵A. W. Overhauser, *Phys. Rev.* **167**, 691 (1968).
⁶H. W. Myron, J. Rath, and A. J. Freeman (unpublished).
⁷F. J. Di Salvo, B. G. Bagley, J. M. Voorhoeve, and J. V. Waszczak, *J. Phys. Chem. Solids* **34**, 1357 (1973).
⁸F. J. Di Salvo, R. G. Maines, and J. V. Waszczak, *Solid State Commun.* **14**, 497 (1974).
⁹J. F. Revelli, Jr. and W. A. Phillips, *J. Solid State Chem.* **9**, 176 (1974).
¹⁰L. J. Van der Pauw, *Phillips Tech. Rev.* **20**, 220 (1958).
¹¹F. J. Di Salvo, A. Menth, J. V. Waszczak, and J. Tauc, *Phys. Rev. B* **6**, 4574 (1972); B. G. Bagley, F. J. Di Salvo, and J. V. Waszczak, *Solid State Commun.* **11**, 89 (1972).
¹²F. J. Di Salvo, *Low Temp. Phys. LT-13* **3**, 417 (1972).
¹³D. E. Moncton and J. D. Axe (unpublished).
¹⁴R. Brouwer and F. Jellinek, *Mat. Res. Bull.* **9**, 827 (1974).
¹⁵P. M. Williams, G. S. Parry, and C. B. Scruby, *Phil. Mag.* **29**, 695 (1974); C. B. Scruby, P. M. Williams, and G. S. Parry, *Philos. Mag.* **31**, 225 (1975).
¹⁶J. C. Phillips, *Phys. Rev. Lett.* **29**, 1551 (1972).
¹⁷J. E. Rowe and J. C. Phillips, *Phys. Rev. Lett.* **32**, 1315 (1974).
¹⁸A. H. Thompson, K. R. Pisharody, and R. F. Koehler, *Phys. Rev. Lett.* **29**, 163 (1972).
¹⁹A. H. Thompson, F. R. Gamble, and J. F. Revelli, *Solid State Commun.* **9**, 981 (1971).
²⁰J. A. Benda, *Phys. Rev. B* **10**, 1409 (1974).
²¹D. J. Huntley and R. F. Frindt, *Can. J. Phys.* **52**, 861 (1974).
²²T. H. Geballe, *Superconductivity in d and f Band Metals*, edited by D. H. Douglass (A.I.P., New York, 1972), No. 4.
²³R. D. Barnard, *Thermoelectricity in Metals and Alloys* (Wiley, New York, 1972).
²⁴H. W. Myron and A. J. Freeman, *Phys. Rev. B* **11**, 2735 (1975).
²⁵K. R. Pisharody, Ph.D. thesis (University of Minnesota), Microfilm No. 71-19, 799 (1970) (unpublished).
²⁶A. J. Grant, T. M. Griffiths, G. D. Pitt, and A. D. Yoffe, *J. Phys. C* **7**, L249 (1974).
²⁷A. H. Thompson, *Phys. Rev. Lett.* **34**, 520 (1975).
²⁸D. W. Murphy, F. J. Di Salvo, G. W. Hull, Jr., J. V. Waszczak, S. F. Meyer, G. R. Stewart, S. Early, J. V. Acrivos, and T. H. Geballe, *J. Chem. Phys.* **62**, 967 (1975).
²⁹W. L. McMillan, *Phys. Rev.* **B**, (to be published).
³⁰D. E. Moncton, J. D. Axe, and F. J. Di Salvo, *Phys. Rev. Lett.* **34**, 734 (1975).



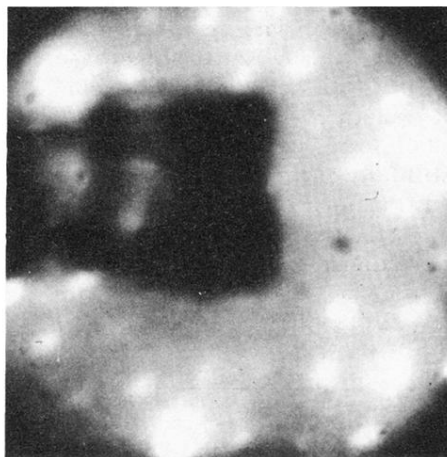
(a) SAMPLE HOLDER



(b) 2H-TaSe₂



(c) 1T-TaSe₂



(d) 1T-TaS₂

FIG. 3. LEED patterns (300 °K). (a) shows the sample holder in front of the fluorescent screen — the holder obscures the central portion of the diffraction pattern in b-d.